ELECTRON PARAMAGNETIC RESONANCE OF THE V^{3+} ION IN $CsAl(SO_4)_2 \cdot 12H_2O$

James G. Clarke

A THESIS

in

The Department

of

Physics

Presented in Partial Fulfillment of the Requirements for

the Degree of Master of Science at

Sir George Williams University

Montreal, Canada

September, 1971

Table of Contents

ABSTRACT

ELECTRON PARAMAGNETIC RESONANCE

OF THE V^{3+} ION IN $CsAl(SO_4)_2 \cdot 12H_2O$

by

James G. Clarke

The electron paramagnetic resonance spectrum of the V^{3+} ion in $CsAl(SO_4)_2 \cdot 12H_2O$ single crystals has been studied in the [111] direction, {100} and {111} planes at 4.2°K with an X-band microwave spectrometer.

The spectrum indicates that the V^{3+} ions have four equivalent sites in a unit cell with the axis of trigonal symmetry of each $[V \cdot 6H_2O]^{3+}$ complex oriented along a [111] direction.

A single broad line is observed from each complex site; the line consists of eight equidistant components which correspond to a nuclear spin I = 7/2 for V^{51}. The resonance spectrum for each complex was interpreted with a spin Hamiltonian of the form

$$H_S = g_{\parallel} H_Z S_Z + A S_Z I_Z$$

The average value of the parameters which gave the best fit to the experimental data were

$$A = (1.027 \pm .005) \times 10^{-2} cm^{-1} \qquad g_{\parallel} = 1.980 \pm .002$$

Acknowledgements

The author wishes to thank Dr. J.A. Mackinnon for suggesting this thesis problem and for his continued aid and encouragement throughout the course of research.

A special note of thanks to Mr. L. Barbopoulos for his useful discussions and constructive criticisms.

Abstract

The electron paramagnetic resonance spectrum of the V^{3+} ion in $CsAl(SO_4)_2 \cdot 12H_2O$ single crystals has been studied in the [111] direction, {100} and{111} planes at $4.2^{o}K$ with an X-band microwave spectrometer.

The spectrum indicates that the V^{3+} ions have four equivalent sites in a unit cell with the axis of trigonal symmetry of each $[V \cdot 6H_2O]^{3+}$ complex oriented along a [111] direction.

A single broad line is observed from each complex site; the line consists of eight equidistant components which correspond to a nuclear spin I = 7/2 for V^{51}. The resonance spectrum for each complex was interpreted with a spin Hamiltonian of the form

$$H_S = g_{\parallel} H_Z S_Z + A S_Z I_Z$$

The average value of the parameters which gave the best fit to the experimental data were

$$A = (1.027 \pm .005) \times 10^{-2} cm^{-1} \qquad g_{\parallel} = 1.980 \pm .002$$

Introduction

The free V^{3+} ion which has a $^3F_2$ ground state contains two unpaired 3d electrons. In the experiment performed by the author, the trivalent vanadium ion replaces an aluminum ion in a single crystal of $CsAl(SO_4)_2 \cdot 12H_2O$. Six H_2O molecules surround the V^{3+} ion forming a near-regular octahedron (Figure 8) which produces a cubic electrostatic crystal field with a small admixture of fields having a lower order of symmetry. In CsAl alum, the field of lower order symmetry has been found by x-ray analysis to be a small trigonal distortion. This trigonal field component appears to have its main origin in the position of the $(SO_4)^{2-}$ groups.

The ground level of V^{3+} ion possesses seven-fold orbital degeneracy (L = 3). The cubically symmetric field removes the orbital degeneracy and converts this level into a singlet and two triplets (Figure 2). The orbital singlet level lies uppermost. The comparatively smaller trigonal field component splits each of the two triplets into a singlet and a doublet. The lower lying singlet level is triple spin degenerate (S = 1). This spin triplet level is further split into a singlet and a doublet through spin-orbit interaction.

Since at low temperatures only the lowest energy levels are occupied, one is interested in only the above three lowest spin levels with which an effective spin[1] S' = 1 can be associated. A Paramagnetic Resonance Spectrometer was used to observe transitions between these three spin levels. Because of the large initial splitting of levels E_1 and $E_{2,3}$ (Figure 3), observation of

absorption lines representing the transitions $E_1 \leftrightarrow E_2$ and $E_1 \leftrightarrow E_3$ ($|\Delta m| = 1$) would require $\sim$7-cm^{-1} quanta. For 1-cm^{-1} quanta a magnetic field of $\sim$60 kilogauss is required. Within the frequency range of $\sim$9300 megacycles and magnetic field values between 100 gauss and 5 kilogauss, one therefore can expect to observe transitions between the upper levels E_2 and E_3 ($|\Delta m| = 2$).

Chapter 1

Theory

1.1 The General Hamiltonian of the Free Vanadium Ion

When an ion is placed in a crystal lattice of given symmetry, the energy levels of the ion are modified by the crystal surroundings. In order to understand these modifications, it is important to review the interactions involved within a free ion.

In the absence of an external magnetic field, the complete Hamiltonian operator is

$$H = T + V_C + V_{SO} + V_{SS} + V_N + V_q \qquad (1)$$

The first term T is the total kinetic energy of the electrons given by

$$T = \sum_k (\vec{P}_k^2 / 2M_o) \qquad (2)$$

where $\vec{P}_k$ is the linear momentum of the kth electron.

M_o is the mass of the electron.

The summation is extended over the index k designating each electron of the system.

The coulomb term V_C consists of

$$V_C = - \sum_k \frac{Ze^2}{r_k} + \sum_{k>j} \frac{e^2}{r_{kj}} \qquad (3)$$

where r_k is the radius vector extending from the nucleus to the electron. In this equation and the following the C.G.S. system of units was used.

r_{kj} is the distance between the k^{th} electron and the j^{th} electron.

The first term in the above equation (3) is the coulomb attraction between the nucleus and the electrons. The expression is summed over all N electrons. The second term represents the coulomb repulsion between electrons and is summed over pairs of electrons.

The next most important interaction is the potential energy due to the spin-orbit coupling between the electron spin $\vec{s}_k$ with orbital momentum $\vec{l}_k$.

$$V_{SO} = \sum_{jk} \left[a_{jk} \vec{l}_j \cdot \vec{s}_k + b_{jk} \vec{l}_j \cdot \vec{l}_k + c_{jk} \vec{s}_j \cdot \vec{s}_k \right] \tag{4}$$

where a_{jk}, b_{jk}, c_{jk} are constants.

In the above formula, k and j range over all electrons. If we confine ourselves to Russel-Saunders coupling, then

$$\sum \vec{l}_j = \vec{L} \tag{5}$$

and

$$\sum \vec{s}_k = \vec{S} \tag{6}$$

The vectors $\vec{L}$ and $\vec{S}$ couple to give the total angular momentum

$$\vec{J} = \vec{L} + \vec{S} \tag{7}$$

The spin-orbit interaction can be written as

$$V_{SO} = \lambda \vec{L} \cdot \vec{S} \tag{8}$$

where λ is the spin-orbit coupling constant for a given ion.

The fourth term of equation (1), V_{SS}, represents the magnetic dipole interaction between electrons.

This term is

$$V_{SS} = \sum_{jk} \frac{1}{r_{jk}^3}\left[\vec{s}_j\cdot\vec{s}_k - \frac{3(\vec{r}_{jk}\cdot\vec{s}_j)(\vec{r}_{jk}\cdot\vec{s}_k)}{r_{jk}^2}\right] \qquad (9)$$

The summation in the above term (9) as in the case of the coulomb repulsion term (3) is extended over all pairs of electrons.

If the nucleus has a spin I and a quadrupole moment Q, the various terms are split again by two additional interactions, V_N and V_q where

$$V_N = 2\gamma\beta\beta_N\left[\sum_k\left\{\frac{(\vec{l}_k-\vec{s}_k)\cdot\vec{I}}{r_k^3} + \frac{3(\vec{r}_k\cdot\vec{s}_k)(\vec{r}_k\cdot\vec{I})}{r_k^5}\right\} + \frac{8\pi\delta}{3}(r_k)(\vec{s}_k\cdot\vec{I})\right] \qquad (10)$$

and

$$V_q = \frac{e^2Q}{2I(2I-1)}\left[\sum_k \frac{I(I+1)}{r_k^3} - \frac{3(\vec{r}_k\cdot\vec{I})^2}{r_k^5}\right] \qquad (11)$$

where l is the orbital angular momentum of an electron

s is its spin

β the Bohr magneton

β_n the nuclear magneton

γ the nuclear gyromagnetic ratio in units of $e/2M_c$

Q the quadrupole moment and

r_k is the distance between the electron and the nucleus.

The first term in the curly brackets in V_N describes the dipole-dipole interaction between the nuclear moment and the magnetic moments of the electron. The second term, containing the delta-function δ, denotes the anomalous interaction of the s-electron with

the nuclear spin. The expression V_q describes the electrostatic interaction with the quadrupole moment Q of the nucleus.

The order of magnitude of these interactions can be estimated from the observed atomic spectra. The level separations of V_C are usually of the order 10^{+5} cm^{-1}, V_{SO} causes splittings of the order 10^{+2} cm^{-1}, $V_{SS} \sim 1$ cm^{-1}, $V_N \sim 10^{-1}$ to 10^{-3} cm^{-1}, $V_q \sim 10^{-3}$ cm^{-1}.

1.2 The General Hamiltonian of Trivalent Vanadium in a crystal lattice and an external magnetic field

When an ion is placed in a crystal lattice, additional terms representing the effects of the lattice on the motion of the electrons must be introduced in the general Hamiltonian for the free ion.

The term V_X, which represents the interaction of the ion and the crystal's electrostatic field is as follows

$$V_X = - \sum_k e_k \phi(r_k) \tag{12}$$

where the summation is extended over all electrons.

When the crystal containing the ion under study is subjected to an external magnetic field, two new terms must also be added to the Hamiltonian for the free ion. The first term which describes the electronic interaction with the external magnetic field H is given by

$$V_H = \sum_k \beta(\vec{l}_k + 2\vec{s}_k)\cdot\vec{H} \tag{13}$$

where β is the Bohr magneton.

The second term gives the direct interaction of the nucleus with

the external field H as follows

$$V_h = -\gamma\beta_N \vec{H}\cdot\vec{I} \tag{14}$$

where γ is the nuclear gyromagnetic ratio

β_N is the nuclear magneton.

The order of magnitude of the above interactions are estimated to be $V_H \sim 1\ cm^{-1}$ while for $V_h \sim 10^{-3}\ cm^{-1}$. The term V_X causes splitting of the order $10^3\ cm^{-1}$ or greater.

The general Hamiltonian for trivalent vanadium under the influence of a crystal field and an external magnetic field is then given by the sum of these interactions

$$H = H_1 + V_H + V_h + V_X \tag{15}$$

where $$H_1 = T + V_C + V_{SO} + V_{SS} + V_N + V_q \tag{16}$$

In the above expression for the general Hamiltonian of trivalent vanadium, the first two terms T and V_C are spin independent. If these terms are neglected, the total general spin Hamiltonian of trivalent vanadium ion under the influence of a crystal lattice may be written as

$$H_S = V_{SO} + V_{SS} + V_N + V_q + V_H + V_h + V_X \tag{17}$$

where the potential energy terms are defined as previous. It is justifiable to drop the spin independent terms from the spin Hamiltonian, since they shift all levels equally and so do not enter into the energy differences.

The spin Hamiltonian [7] applicable to V^{3+} is given by

$$H_S = g_{\parallel}\beta H_Z S_Z + g_{\perp}(H_X S_X + H_Y S_Y) + D(S_Z^2 - 2/3)$$
$$+E(S_X^2 - S_Y^2) + AI_Z S_Z + B(I_X S_X + I_Y S_Y) \qquad (18)$$

The effective spin Hamiltonian to interprete the spectrum of V^{3+} ions in CsAl alum may be obtained from equation (18), by deleting those terms that give only off diagonal elements and also by omitting the axial field DS_Z^2, which is the same for both $m = \pm 1$. This Hamiltonian is of the form

$$H_S = g_{\parallel}\beta H_Z S_Z + AS_Z I_Z \qquad (19)$$

where $g_{\parallel}$ is the g-factor parallel to the trigonal axis

β is the Bohr-magneton

A is the hyperfine-splitting constant.

The value of the magnetic field for the position of the m^{th} hyperfine component is given by

$$H_m = (h\nu - Am)/g_{\parallel}\beta\cos\theta) \qquad (20)$$

where h is planck's constant

ν is the frequency of the microwave source

θ is the angle between the magnetic field H_m and the trigonal axis of the $[V \cdot 6H_2O]^{3+}$ complex.

1.3 The expressions for the magnetic field for resonance in the {100} and {111} planes.

The magnetic field value at this point of resonance for the m^{th} hyperfine component, may be obtained from

$$H_m = (\tfrac{1}{2}h\gamma - Am)/g_{\parallel}\beta\cos\theta) \qquad (21)$$

where θ is the angle between the magnetic field H_m and the trigonal axis. This expression must be modified to allow for movement of the magnetic field H in the {100} and {111}planes. As a preliminary to this calculation, a few solid geometry relationships must be considered.

Suppose that the paramagnetic resonance experiment was performed first in the {111} plane. The relationship between the angle θ (the angle between the complex symmetry axis and H_{dc}) and θ_r (the angle between H_{dc} and some reference line r in the {111} plane) is required (Figure 4a). To obtain this relationship one must consider figure 4b where

$$\cos(c) = \cos(a)\cdot\cos(b) + \sin(a)\cdot\sin(b)\cdot\cos(c) \qquad (22)$$

Using the above spherical geometry formula and the following equivalents $c = \theta$; $a = \theta_H$; $b = 19^o18'$ and $c = 90^o$; the relationship between θ and θ_H is found to be

$$\cos(\theta) = 0.94284\cos(\theta_r) \qquad (23)$$

If one considers figures 5a and 5b a similar relationship can be found for experiments in which H_{dc} is in the {100} plane.

This expression is

$$\cos(\theta) = 0.81647 \cos(\theta_r) \tag{24}$$

The expressions for the magnetic field for resonance in the {100} and {111} planes then become

$$\cos(\theta) = 0.81647 \cos(\theta_r) \tag{25}$$

and

$$\cos(\theta) = 0.94284 \cos(\theta_r) \tag{26}$$

Chapter 2

Crystallography

The crystal structure of the alums can be summarized as a series of double salts[8] with the formula

$$R^{i}R^{iii}(R^{vi}O_4)_2 \cdot 12H_2O$$

in which R^{i} is a monovalent metal, R^{iii} is a trivalent metal, and R^{vi} is either a sulfur, selenium or tellurium. The crystals belong to the pyrotehedral class of the cubic system, with four molecules of the above form per unit cell. More specifically, the space group is T_h^6 (Pa3) while the point group is $T_h(\frac{2}{m}\,\bar{3})$. In the author's case, the alum used in the Electron Paramagnetic Resonance experiment was $CsAl(SO_4)_2 \cdot 12H_2O$.

The relative positions of the various atoms are shown in Figure 1. The metal cations occupy alternate sites on the cube corners. In all known cases, six H_2O molecules are octahedrally coordinated with the small trivalent cations (Figure 8). If the vanadium ion is assumed to be at the point (o,o,o), the ligand ions may be taken to be approximately at the points

$$(\pm a,\ o,\ o),\ (o,\ \pm a,\ o),\ (o,\ o,\ \pm a)$$

thus forming a regular octahedron.

The distribution of the other six H_2O molecules depends on the size of the monovalent ions, and to some extent characterizes the α, β and γ alum types. The CsAl alum used in this experiment is classified as a β alum. The eight $(SO_4)^{2-}$ groups are dispersed equally through the different octants of the unit cell and consists

of a single sulfur atom surrounded by four tetrahedrally coordinated oxygens. The bonding arrangement in a single octant, shown in Figure 1, is typical for β or α alum.

Since the crystal field at the R^{3+} site is determined by the arrangement and position of the various ligands, it is appropriate to list the different neighbors in order of proximity

six octahedrally coordinated H_2O	at 2.0A°
six $(SO_4)^{2-}$	at 5.0A°
six R^{1+}	at 6.0A°
two $(SO_4)^{2-}$	at 6.5A°

The location of the sulfate ions which represents the second and fourth neighbors are shown schematically in Figure 7. The six second neighbors lie in {110} planes approximately at the intersections of the line through R^{3+}, which forms a 90° angle with the two parallel octant body diagonals. In each case, that is in Figure 7(a), 7(b), and 7(c) the distance d_o from R^{3+} to S is equal. For the β type alum, d_o is equal to 0.409 a_o where a_o is the lattice constant.

As indicated in Figure 6, the six $(SO_4)^{2-}$ groups form a trigonally distorted octahedron around R^{3+}, with the threefold axis of symmetry along a unit cell [111] direction. On this same axis but outside of the distorted octahedron, the remaining two sulfates lie at a distance d_o' equal to $0.572a_o$ for a β alum.

In the following table, the values of a_o, d_o, and d_o' are listed for the particular alum crystal used by the author.

Table 1

Crystal-Structure data

Alum	Type	a_o	d_o	d'_o
$CsAl(SO_4)_2 \cdot 12H_2O$	β	12.333A°	5.044A°	7.054A°

Crystal Preparation

The crystals used in the experiment were prepared by allowing a hot saturated solution of V^{3+} ions in CsAl alum surrounded by a nitrogen atmosphere to cool slowly to room temperature. One sample was later analyzed and found to contain 1.86% vanadium, 4.5% aluminium, while there was 23.6% cesium by weight.

Chapter 3

Experimental Apparatus

The purpose of this section is to briefly describe the Electron Spin Resonance Apparatus used by the author. Figure 9 is a functional block diagram of the principle components of the electron spin resonance spectrometer.

The basic components are: 1) an electromagnet whose homogeneous gap field H can be swept continuously with respect to time from 1 kilogauss to 10 kilogauss; 2) a generator for producing a slow low frequency modulation of 400 Hz of the main field H at the center of the air gap; 3) a stable klystron signal oscillator supplying microwave energy with a frequency of about 9,500 MHz to 4) a sample rectangular cavity resonating at the klystron frequency; 5) a local klystron oscillator to heterodyne the reflected signal from the resonate cavity after resonance; 6) a crystal detector; 7) a graphic recorder.

The X-band microwave bridge contains a klystron, isolator, attenuator and a hybrid tee. The signal klystron oscillator generates microwave energy over the operating frequency range of 8.8 to 9.6 GHz to irradiate the sample. The klystron is coupled to the wave guide system by an attenuator and ferrite isolator. As a unidirectional attenuator, the isolator prevents reflected energy due to a mismatch in the microwave system from affecting the output frequency of the klystron. The isolator provides forward attenuation of less than 1 decibel, with a reverse attenuation of over 30 decibels. In this way, the klystron is affectively isolated from any reflected

power. The microwave energy then passes through a variable attenuator which controls the level of energy applied to the hybrid junction. In addition to controlling the power output, the attenuator also serves to isolate the klystron from unwanted reflected energy.

The microwave bridge's hybrid tee consists of both a low and a high power arm, a 20 dB directional coupler, and a detector arm. The 20 decibel coupler provides a monitoring point for power at the hybrid tee. By observing the power at this point, the variable attenuator may be calibrated. The power entering the hybrid tee from the signal klystron oscillator divides equally between the low and high power arms. The low power configuration is used in the electron spin resonance experiment performed.

The components of this arm are a cryostat isolator, a phase shifter, and a sample resonance cavity. The crystal isolator allows the incident power on the cavity to be adjusted from -6dB to -40dB attenuation in reference to the power from the hybrid junction. The signal reflected from the sample cavity containing the resonance information passes unattenuated back through the cryostat isolator. The phase shifter immediately following the crystal isolator adjusts the phase of the microwave power incident on the sample cavity. The cavity assembly is connected to the phase shifter by a standard (1.27 x 2.54 cm) gold-plated brass wave guide.

The high power arm of the microwave bridge is connected to the X-band superheterodyne adapter unit. The adapter unit's principle components are a local klystron oscillator, a ferrite isolator, and a variable attenuator. The local oscillator is tuned to a

frequency ± 30MHz from the klystron signal oscillator frequency in the microwave bridge. The ferrite isolator, and variable attenuator perform the same function in the adapter unit as in the bridge unit. The local oscillator energy is coupled to the hybrid tee's high power arm by means of a slide screw tuner. This tuner ensures the correct matching between the two systems.

When resonance is obtained at the sample, the cavity impedance is changed and a signal is reflected from the cavity to the detector arm in the hybrid tee. At the crystal detector, the reflected signal is heterodyned with the local oscillator frequency. The 30 MHz difference frequency containing the modulation electron spin resonance information is applied to the pre-amplifier which is attached to the crystal detector. The information signal is then passed through several amplifier units that provide high selectivity, sensitivity and sharp response. From the amplifier stage, the absorption line derivative is displayed on a graphic recorder.

Before outlining the experimental procedure used to obtain the electron paramagnetic resonance spectra of V^{3+} in CsAl alum, something should be said about the dewar vessels used to contain the liquefied gases. As shown in Figure 9, the main dewar is placed between the pole faces of the magnet and contain the microwave cavity with the paramagnetic sample immersed in liquid helium at its boiling temperature of $4.2^{o}K$. In addition, a second dewar containing liquid nitrogen at $77^{o}K$ surrounds the helium dewar, thus providing a radiation shield to conserve the liquid helium more effectively.

Chapter 4

Experimental Procedure

4.1 Initial Preparations

To prepare the system for Electron Spin Resonance experiment at low temperatures, the crystal sample was introduced and oriented on the bottom internal face of the sample cavity. The crystal was held in position by vacuum grease. Also placed in the sample cavity was a small amount of dipheryl picryl hydrazyl (D.P.P.H.) which provided a method to measure the frequency of the klystron. The sample cavity and its waveguide extension were then suspended within the dewar system.

The dewar system (Figure 9) was then placed in such a manner that its lower neck section was centrally positioned between the pole caps of the direct current magnet. By centering the lower section, it was also possible to position the crystal sample at the mid-point between the pole caps. To obtain the experimental temperature of $4.2^{o}K$, it was necessary to use liquid nitrogen and liquid helium. Both liquids were contained and stored by the dewar system which consisted of an inner and outer vessels. The outer vessel has a permanent vacuum jacket while the inner vessel is surrounded by a variable vacuum jacket.

Before introducing liquid nitrogen into the larger outer dewar, the variable vacuum jacket of the inner vessel was flushed several times with dry nitrogen gas. Upon completion of this procedure, the variable vacuum jacket was filled with a small amount of dry nitrogen gas. The sample chamber of the inner dewar was also flushed and filled with dry nitrogen gas. After the introduction of

liquid nitrogen into the outer dewar, the system was allowed to cool for approximately one-half hour stabilizing at liquid nitrogen temperature of $77^{\circ}K$.

When temperature equilibrium of the system had been reached, the sample chamber of the inner dewar was flushed with dry helium gas. Before liquid helium was transferred into this chamber, the variable jacket which previously had been filled with a small amount of dry nitrogen gas was evacuated. The Electron Spin Resonance experiment was able to be performed after the system stabilized at liquid helium temperature of $4.2^{\circ}K$.

4.2 Determination of Absorption Points

After initial preparations of the dewar system were completed, the Paramagnetic Resonance Spectrometer was tuned to detect the single resonance line of D.P.P.H. at a particular magnet angle. By carefully adjusting the spectrometer to determine this resonance condition for D.P.P.H., the set of eight resonance lines for V^{3+} was also detected by varying the value of the magnetic field. As the magnet was rotated about the vertical axis of the sample cavity in intervals of five degrees, a similar set of resonance lines was detected at each angular position.

The data output from the spectrometer at each particular magnet setting was in the form of a first derivative absorption curve. The experimental magnetic field value at each point of energy absorption was determined from this spectrum by two methods to be discussed later. These points of absorption corresponded to the spectrum crossover points on the chart recorder curve (Figure 10).

The justification for taking these crossover points as the actual absorption points was verified upon integrating (appendix I) the first derivative spectrum when the crystal was oriented in the [111] direction. As illustrated in table 2, a small error of 6 gauss was found to exist between the integrated and non-integrated resonance magnetic field values at the points of energy absorption.

4.3 Measurement of Magnetic Field Values

The experimental magnetic field value at a point of energy absorption for each of the eight hyperfine lines was determined by two methods: 1) by a Nuclear Magnetic Resonance (N.M.R.) fluxmeter, 2) by measuring the position of the resonance signals on the chart recording with a travelling microscope.

4.3.1 Nuclear Fluxmeter Method

The time dependent magnetic field was adjusted slowly until a resonance signal was detected on the chart recorder. At the exact point of absorption which was represented on the chart paper by a crossover point of the first derivative signal, the magnetic field was held constant. The fluxmeter probe was then placed between the magnet pole caps near the sample cavity. After the N.M.R. absorption signal for this steady value of the magnetic field was located on the N.M.R. fluxmeter's oscilloscope, the fluxmeter's transmitter frequency was monitored with an electronic counter. To obtain the value of the magnetic field, the frequency displayed by the counter was multiplied by the constant of the probe used. The Nuclear

Fluxmeter Method was repeated until the magnetic field value for each energy absorption point was determined.

4.3.2 Travelling Microscope Method

The experimental magnetic field values at the points of energy absorption were also determined by the use of a travelling microscope. As mentioned above, at each angular position of the magnet the spectrometer's output on the chart recorder was a first derivative spectrum consisting of eight absorption crossover points. By means of the travelling microscope, the distance from a common line which was chosen as the initial magnetic field sweep point on the chart paper, to an absorption crossover point was measured. Similarly, the total distance between the initial magnetic field sweep point or common line and the final magnetic field sweep point on the chart recorder paper was determined. The ratio of the first measurement to the second was then formed. The experimental magnetic field value at the point of resonance was calculated by multiplying this ratio by the total value of the magnetic field sweep in gauss. This procedure was then repeated for each absorption point.

4.4 Measurement of Klystron Frequency

The klystron frequency was determined by means of a small amount of D.P.P.H. which was included in the sample cavity. The microwave frequency is given by

$$\gamma = g\beta H/h$$

where g is the landé splitting factor for D.P.P.H.

β is the Bohr Magneton

h is Planck's constant

H is the magnetic field value at the point of resonance for D.P.P.H

The value of the magnetic field H in the above formula was obtained by means of a Nuclear Magnetic Resonance Fluxmeter. When the following sample numerical values g = 2.0037 (D.P.P.H.), $\beta = 9.2732 \times 10^{-21}$ ergs/sec, $h = 6.625 \times 10^{-27}$ ergs/sec. and H = 3.322 Kilogauss were substituted into the above formula, the klystron frequency was found to be 9318 megacycles/sec.

Chapter 5

Data Analysis

In order to analyse the experimental data consisting of the magnetic field values which were obtained from the first derivative absorption curve, two methods were used: 1) a ratio method which employed a minimum set of resonance field values; 2) a least square fitting method that compared the theoretical and experimental resonance field values for each angular position of the magnet.

5.1 The Ratio Method

(1) To determine the constants A and $g_{\parallel}$ in equation (20), a ratio of the set of minimum field values was formed as follows

$$\frac{H_m}{H_{m'}} = \frac{(1/2h\gamma - A\cdot m)}{(1/2h\gamma - A\cdot m')} \tag{27}$$

where m and m' refer to the nuclear spin quantum numbers and H_m and $H_{m'}$ are the minimum magnetic field values corresponding to nuclear spin quantum numbers m and m'.

The hyperfine constant A is then determined by

$$A = \frac{h\gamma(1-b)}{A' - B'b} \tag{28}$$

where b is the ratio of H_m to $H_{m'}$.

The g-factor parallel to the trigonial axis is determined by

$$g_{\parallel} = \frac{1/2h\gamma - A\cdot m}{H_m \beta \cos\theta} \tag{29}$$

where A was previously determined from equation (27), and

θ is the angle between the magnetic field H_m and the trigonal axis of the $[V \cdot 6H_2O]^{3+}$.

(2) Average values for A and $g_{\parallel}$ were determined by considering several different combinations of the eight minimum field values in the ratio for b.

5.2 The Least Square Fitting Method

(1) The magnetic field values which were determined either by a travelling microscope or by the nuclear fluxmeter were plotted versus magnet angle (Figure 11). The magnet angle for which the line spectrum of each of the eight components was a minimum, was determined. To obtain this angle, two procedures were used and compared. The first procedure was by observing the above graph while the second method employed a polynomial curve fit of degree ten. An average minimum angle was then calculated from the above procedures.

(2) A corrected set of experimental angles were then obtained when this average minimum field angle was subtracted from the original magnet angles (Table 3).

(3) By a least square fitting technique, that compared the corrected set of experimental data consisting of the original field values and the corresponding corrected experimental angles and the theoretical data calculated from equation 20, the values of the constant $g_{\parallel}$ and A were determined.

(4) A three dimensional graph was plotted to illustrate that the parameter values were minimum.

Chapter 6

Results and Discussion

The experimental magnetic field results obtained from the Nuclear Fluxmeter and Travelling Microscope Methods for different crystal planes and directions are listed in tables 3, 5, 7, 8, 9 and 10. The corresponding theoretical magnetic fields calculated by Equation (20) which was modified by the crystal plane correction factors are listed in Tables 4 and 6. The values of the parameters A and $g_{//}$ obtained from the Ratio Method and the Least Square Fitting Method are given in Table 11 along with the average values for these parameters.

As shown in Table 11, it was impossible to reproduce in different experimental runs identical parameter values for a given signal. This slight variation was due to difficulties encountered in orienting the crystals in the microwave cavity. The limited range of the parameter values for different crystal planes and directions illustrated that the Ratio and Least Square Fitting Methods were comparative.

At liquid nitrogen and room temperatures, the V^{3+} spectrum was not detected. At liquid helium temperature a single broad line was observed for each complex site; the line consisted of eight equidistant components which correspond to a nuclear spin I = 7/2 for V^{51}. The spectrum indicates that the V^{3+} ions have four equivalent sites in a unit cell with the axis of trigonal symmetry of each $[V \cdot 6H_2O]^{3+}$ complex oriented along the [111] direction. The maximum energy absorption occured when the sample was placed in the cavity so that the rf magnetic field was parallel to the static magnetic field. This indicates that the transition under study is the one for $|\Delta m| = 2$

The angular dependence of the eight hyperfine lines for both the {111} plane and the {100} plane is illustrated in Figure 11 and 12. As the magnet angle increased, the separation between the hyperfine components remained approximately constant. With the magnetic field along the [111] direction (Figure 10), the line width of the single broad line, the line width of each of the eight components, and the separation of each of the eight components was 870, 50, 109 gauss respectively.

The experimental results reported here are in good agreement with those obtained by Zverev and Prokhorov (1960) in their investigation of V^{3+} in single crystals of corundum. Similar results to those reported in Table 10, also were determined by Lambe and Kikuchi (1960).

Appendix I

Integration of Absorption Spectra

The first derivative absorption spectra obtained from the Electron Spin Resonance Spectrometer was integrated by two methods 1) by Simpsom's rule and 2) by the Trapazoid rule. The spectrum was integrated to determine the extent of the error in taking the crossover points of the first derivative curve as the point of absorption. The integration methods were applied to the first derivative spectrum of V^{3+} ion in CsAl alum in the [111] direction as shown in Figure 10.

Simpson's rule to approximate the area of the region bounded by the curve $y = f(x)$, the x-axis, $x = a$ and $x = b$

$$\int_a^b f(x)dx \approx \frac{h}{3}(y_0 + 4y_1 + 2y_2 + 4y_3 + 2y_4 + \ldots\ldots 4y_{n-1} + y_n)$$

where $h = (b-a)/n$.

When the estimated absorption points of the first derivative curve were compared to the calculated absorption points of the integrated curve an average error of 7 gauss was found (Table 2).

The secomd method to integrate the first derivative absorption curve was the Trapezoidal rule defined by

$$\int_a^b f(x)dx = \frac{\Delta_x}{2}\left[f(x_0) + 2f(x_1) + 2f(x_2) + \ldots\ldots + 2f(x_{n-1}) + f(x_n)\right]$$

where $\Delta x = (b-a)/n$

and $x_i = a + i\Delta x$

The average error for this method was found to be 5 gauss (Table 2)

Bibliography

1. Abragam, A., Pryce, M.H.L., Proc. Roy. Soc., A205, 135, 1951.
2. Al'tahuler, S.A., Kozyrev, B.M., Electron Paramagnetic Resonance. New York: Academic Press, 1964.
3. Assenheim, H.M., Introduction to Electron Spin Resonance. New York: Plenum Press, 1967.
4. Ballhausen, C.J., Introduction to Ligand Field Theory. New York: McGraw-Hill Book Co., 1962.
5. Chakravarty, A.S., Proc. Phys. Soc., A74, 711, 1959.
6. Dionne, G.F., Ph.D. Thesis (unpublished), McGill Univ., 1964.
7. Lambe, J., Kikuchi, C., Phys. Rev., 113, 71, 1959.
8. Lipson, H., Proc. Roy. Soc., 151, 347, 1935.
9. Low, W., Paramagnetic Resonance in Solids. New York: Academic Press, 1960.
10. Macfarlane, R.M., Wong, J.Y., 166, 251, 1967.
11. Mackinnon, J.A., Ph.D. Thesis (unpublished), McGill Univ., 1968.
12. Mackinnon, J.A., Dionne, G.F., Can. J. Phys., 44, 2329, 1966.
13. Mackinnon, J.A., Dionne, G.F., Phys. Rev., 172, 325, 1968.
14. Mackinnon, J.A., Manoogian, A., Can. J. Phys., 45, 2769, 1967.
15. McMillan, J.A., Electron Paramagnetism. New York: Reinhold Book Corporation, 1968.
16. Pake, G.E., Paramagnetic Resonance. New York: W.A. Benjamin Inc., 1962.
17. Rêi, D.K., Soviet Phys. - Solid State, 3, 1606, 1961.
18. Rozenburg, H.M., Low Temperature Solid State Physics. London: Oxford Univ. Press, 1965.

19. Squires, T.L., An Introduction to Electron Spin Resonance. New York: Academic Press, 1964.

20. Van Vleck, J.H., The Theory of Electric and Magnetic Susceptibility. London: Oxford Univ. Press, 1923.

21. Van Vleck, J.H., J. Chem. Phys., 7, 61, 1939.

22. Yastrebov, V.N., Soviet Phys. - Solid State, 9, 95, 1966.

23. Zverev, G.M., Prokhorov, A.M., Soviet Physics JETP, 34, 1023, 1958.

24. Zverev, G.M., Prokhorov, A.M., Soviet Physics JETP, 11, 330, 1960.

Table 2

Absorption Magnetic Field Values

Magnetic Field Values by Simpson's Rule in gauss	Magnetic Field Values by Trapazoid Rule in gauss	Magnetic Field Values by Nuclear Fluxmeter in gauss
1278	1287	1287
1380	1385	1390
1494	1499	1503
1608	1612	1612
1721	1721	1725
1830	1830	1834
1940	1940	1944
2044	2048	2053

Table 3

Results of March 5, 1970 {111} plane

Magnet Angle	Corrected Magnet Angle	Experimental Resonance Field Values in Gauss							
		Spin +7/2	Spin +5/2	Spin +3/2	Spin +1/2	Spin -1/2	Spin -3/2	Spin -5/2	Spin -7/2
-40°	-43°	1825	2008	2150	2268	2432	2584	2778	-
-30°	-33°	1619	1761	1893	2030	2164	2284	2427	2564
-20°	-23°	1502	1625	1754	1884	2007	2134	2235	2353
-10°	-13°	1416	1535	1649	1774	1892	2004	2108	2226
0°	-3°	1409	1522	1638	1752	1875	1983	2102	2208
$+10^{\circ}$	$+7^{\circ}$	1426	1544	1668	1785	1897	2013	2131	2232
$+20^{\circ}$	$+17^{\circ}$	1461	1583	1714	1836	1953	2088	2212	2320
$+30^{\circ}$	$+27^{\circ}$	1530	1663	1792	1925	2056	2191	2320	2449
$+40^{\circ}$	$+37^{\circ}$	1728	1875	2019	2155	2287	2442	2586	-
$+50^{\circ}$	$+47^{\circ}$	2053	2202	2388	2568	-	-	-	-

Parameters $g_{\parallel} = 1.985$

$A = 1.010 \times 10^{-2}$ cm.

Table 4

Results of March 5, 1970 {111} plane

Magnet Angle	Theoretical Resonance Field Values in Gauss							
	Spin +7/2	Spin +5/2	Spin +3/2	Spin +1/2	Spin -1/2	Spin -3/2	Spin -5/2	Spin -7/2
-43^{o}	1854	2011	2167	2323	2480	2636	2792	-
-33^{o}	1623	1760	1897	2034	2171	2307	2444	2581
-23^{o}	1484	1609	1734	1859	1984	2109	2234	2359
-13^{o}	1406	1524	1643	1761	1880	1998	2117	2235
$-\ 3^{o}$	1376	1492	1607	1723	1839	1955	2071	2187
$+\ 7^{o}$	1388	1505	1622	1739	1856	1973	2090	2207
$+17^{o}$	1446	1567	1689	1811	1933	2055	2177	2298
$+27^{o}$	1558	1689	1820	1951	2083	2214	2345	2476
$+37^{o}$	1746	1893	2040	2188	2335	2482	2629	-
$+47^{o}$	2058	2232	2405	2579	-	-	-	-

Table 5

Results of October 10, 1970 {100} plane

Magnet Angle	Corrected Magnet Angle	Experimental Resonance Field Values in Gauss							
		Spin +7/2	Spin +5/2	Spin +3/2	Spin +1/2	Spin -1/2	Spin -3/2	Spin -5/2	Spin -7/2
-25°	-23°	1699	1890	2039	2187	2341	-	-	-
-20°	-18°	1646	1794	-	2085	2212	2360	-	-
-15°	-13°	1616	1750	-	2029	2164	2300	2441	2571
-10°	- 8°	1590	1720	1863	1997	2138	2268	2406	2532
- 5°	- 3°	1570	1716	1855	1992	2120	2258	2387	2519
0°	2°	1539	1723	1865	-	2143	2269	2401	2527
+ 5°	+ 7°	1593	1729	1868	2002	2141	2269	2405	2525
+10°	+12°	1626	1761	-	2042	2176	2314	2449	2586
+15°	+17°	1642	1791	-	2080	2227	2369	2519	2655
+20°	+22°	1719	1871	2029	2167	2317	-	-	-

Parameters $g_{\parallel} = 1.980$

$A = 1.030 \times 10^{-2}$ cm

Table 6

{100} plane

Magnet Angle	Theoretical Resonance Field Values in Gauss							
	Spin +7/2	Spin +5/2	Spin +3/2	Spin +1/2	Spin -1/2	Spin -3/2	Spin -5/2	Spin -7/2
-23^{o}	1706	1853	2000	2148	2295	-	-	-
-18^{o}	1653	1796	-	2082	2224	2367	-	-
-13^{o}	1616	1756	-	2035	2174	2314	2453	2599
-8^{o}	1592	1730	1867	2005	2142	2280	2417	2555
-3^{o}	1581	1718	1854	1991	2128	2264	2401	2537
$+2^{o}$	1583	1719	1856	-	2129	2266	2402	2539
$+7^{o}$	1596	1734	1871	2009	2147	2285	2423	2560
$+12^{o}$	1622	1762	-	2042	2182	2322	2462	2602
$+17^{o}$	1662	1805	-	2092	2236	2379	2523	2666
$+22^{o}$	1717	1865	2014	2162	2310	-	-	-

Table 7

Results of October 26, 1970 [111] direction

Spin Values	Corresponding Resonance Field Values in Gauss	
+7/2	1287	
+5/2	1390	
+3/2	1503	$A = 1.019 \times 10^{-2} cm^{-1}$
+1/2	1612	$g_{\parallel} = 1.984$
-1/2	1725	
-3/2	1834	
-5/2	-	
-7/2	-	

Table 8

Results of September 17, 1970 [111] direction

Spin Values	Corresponding Resonance Field Values in Gauss	
+7/2	1290	
+5/2	1397	
+3/2	1512	$A = 1.019 \times 10^{-2} cm^{-1}$
+1/2	1619	$g_{\parallel} = 1.975$
-1/2	1732	
-3/2	1840	
-5/2	-	
-7/2	-	

Table 9

Results of October 22, 1970 {111} plane

Spin Values	Corresponding Resonance Field Values in Gauss	
+7/2	1368	
+5/2	1487	
+3/2	1605	$A = 1.049 \times 10^{-2} cm^{-1}$
+1/2	1722	$g_{\parallel} = 1.984$
-1/2	1851	
-3/2	-	
-5/2	-	
-7/2	-	

Table 10

Results of November 4, 1970 {100} plane

Spin Values	Corresponding Resonance Field Values in Gauss	
+7/2	1560	
+5/2	1696	
+3/2	1830	$A = 1.032 \times 10^{-2} cm^{-1}$
+1/2	-	$g_{\parallel} = 1.971$
-1/2	2112	
-3/2	2227	
-5/2	2387	
-7/2	2522	

Table 11

Experimental Procedure	Parameter Values for Different Crystal Orientations		
	{111} plane	{100} plane	[111] direction
Travelling Microscope Method	$g_{\parallel} = 1.985$ $A = 1.010 \times 10^{-2} cm^{-1}$		
Fluxmeter Method	$g_{\parallel} = 1.984$ $A = 1.049 \times 10^{-2} cm^{-1}$	$g_{\parallel} = 1.980$ $A = 1.030 \times 10^{-2} cm^{-1}$	$g_{\parallel} = 1.975$ $A = 1.017 \times 10^{-2} cm^{-1}$
		$g_{\parallel} = 1.971$ $A = 1.032 \times 10^{-2} cm^{-1}$	$g_{\parallel} = 1.984$ $A = 1.019 \times 10^{-2} cm^{-1}$
Average Parameter Values	$g_{\parallel} = 1.980 \pm .002$ $A = (1.027 \pm .005) \times 10^{-2} cm^{-1}$		

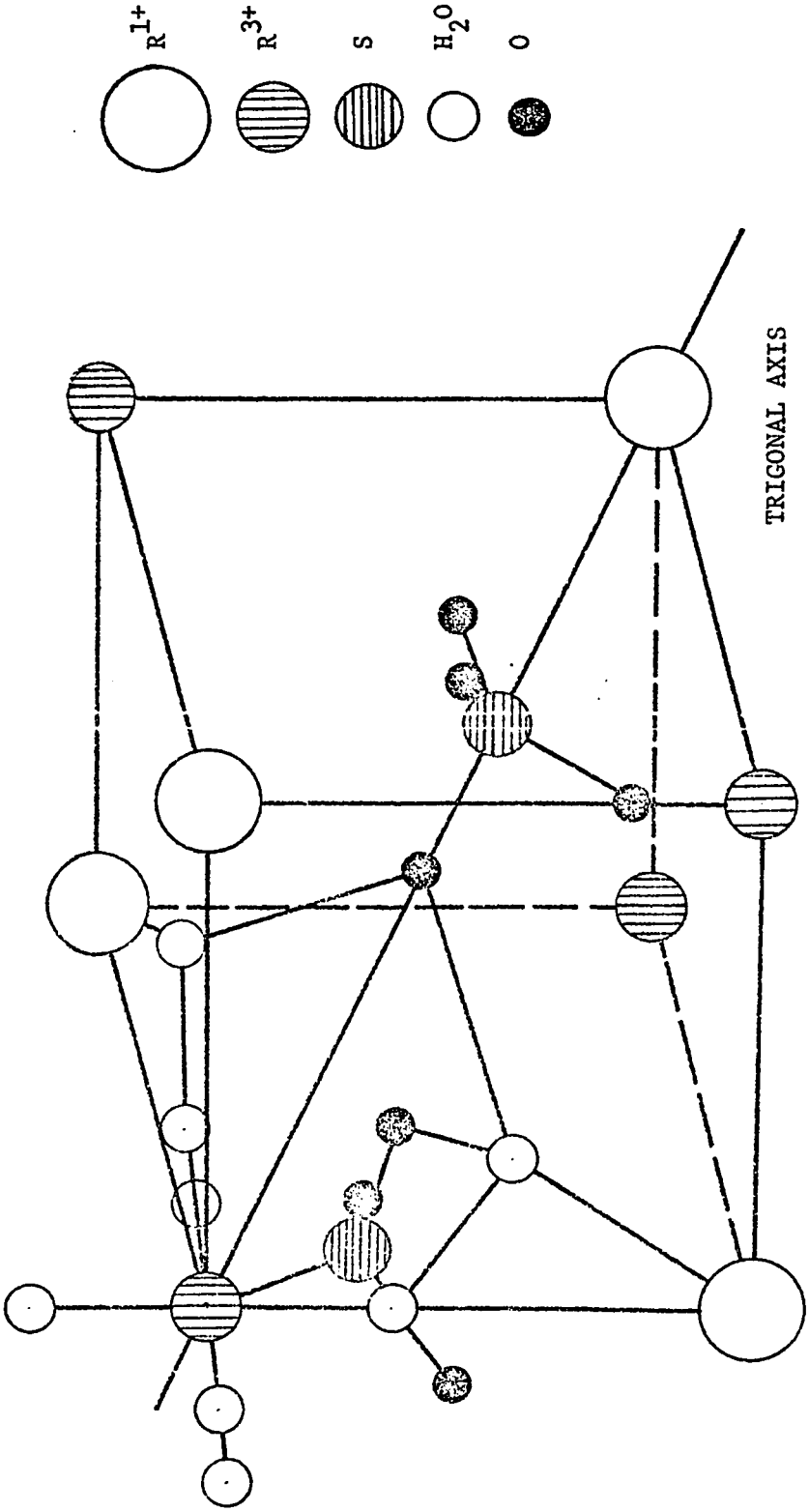

Figure 1. Structure details of one octant of an β-type are shown together with the axis of trigonal symmetry.

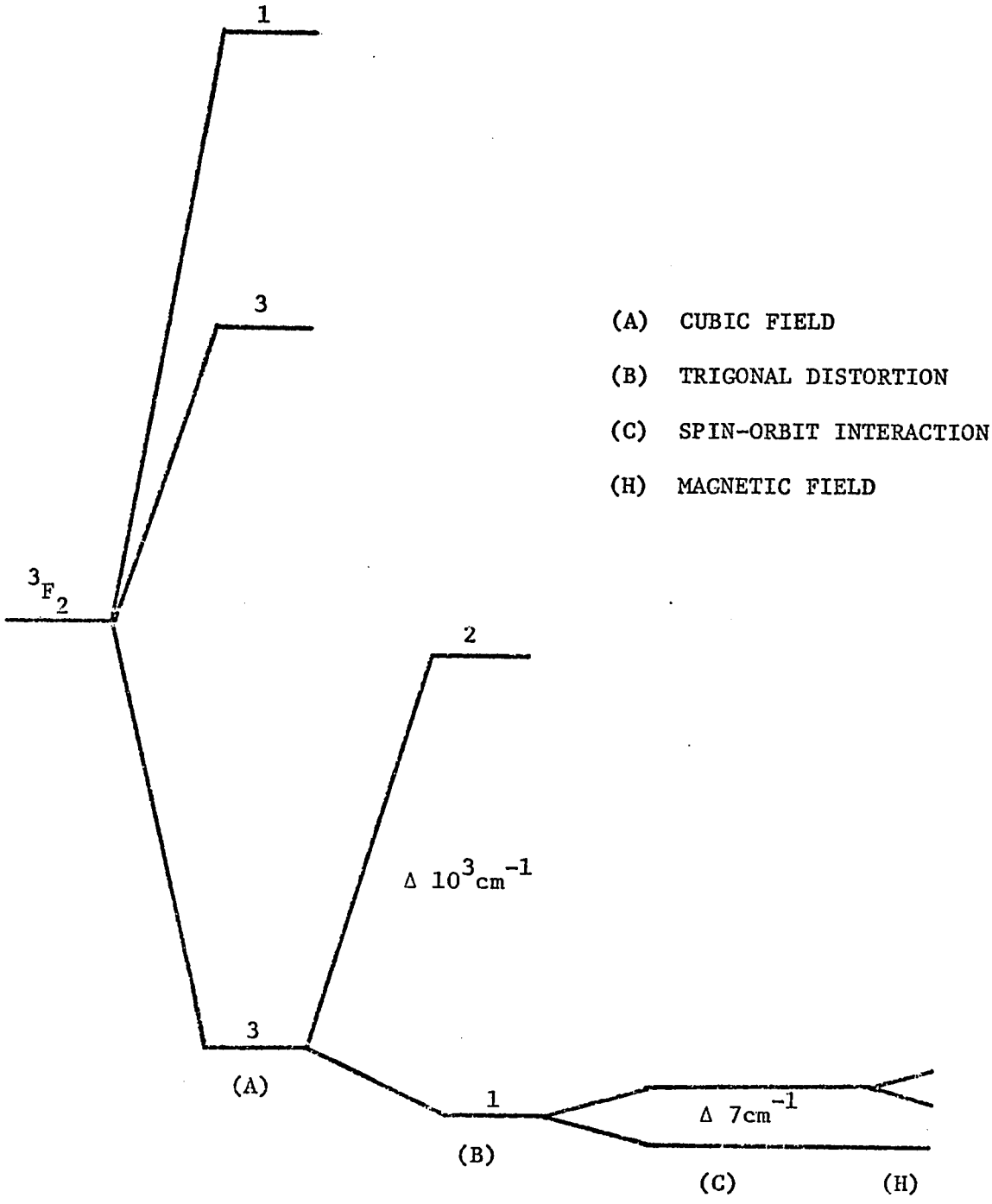

Figure 2. Energy level diagram of vanadium ion in CsAl alum.

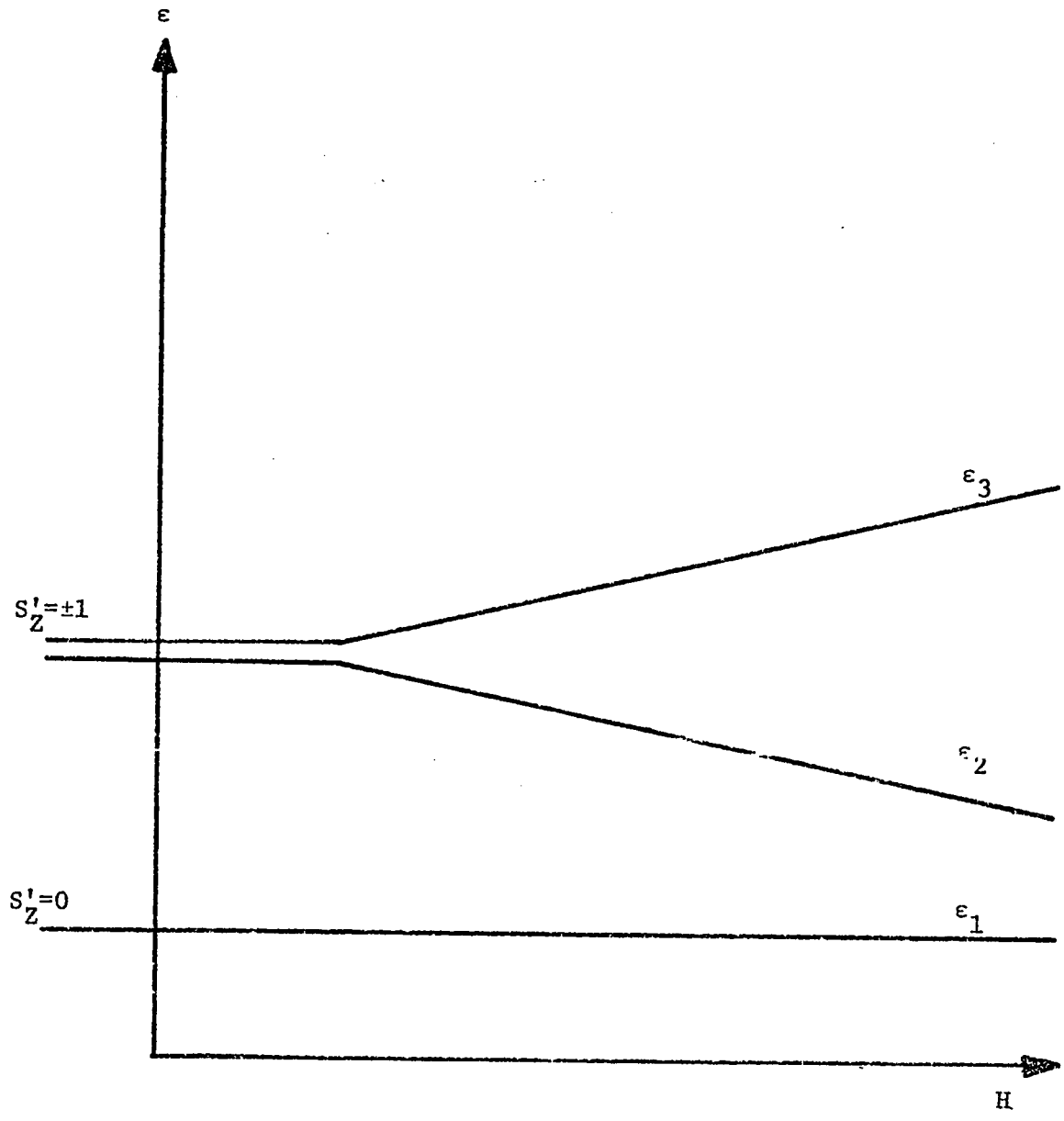

Figure 3. The three lowest spin levels, with which we can associate the effective spin S' = 1.

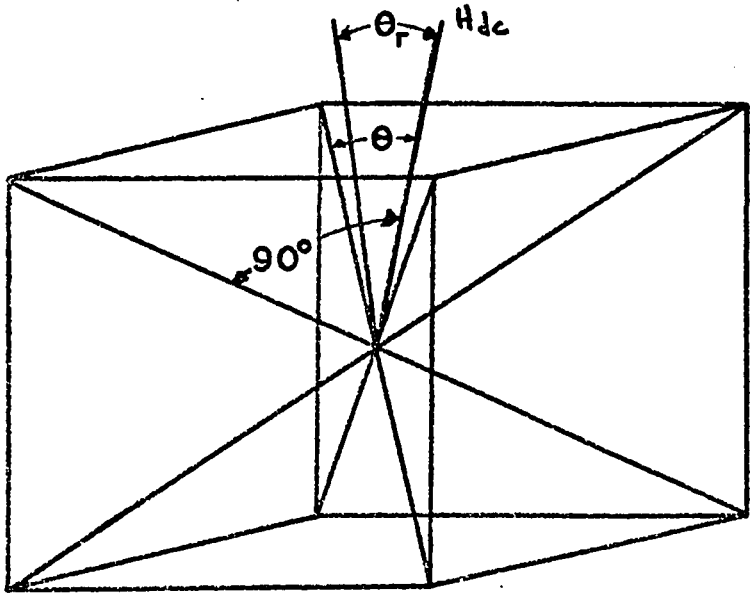

Figure 4a

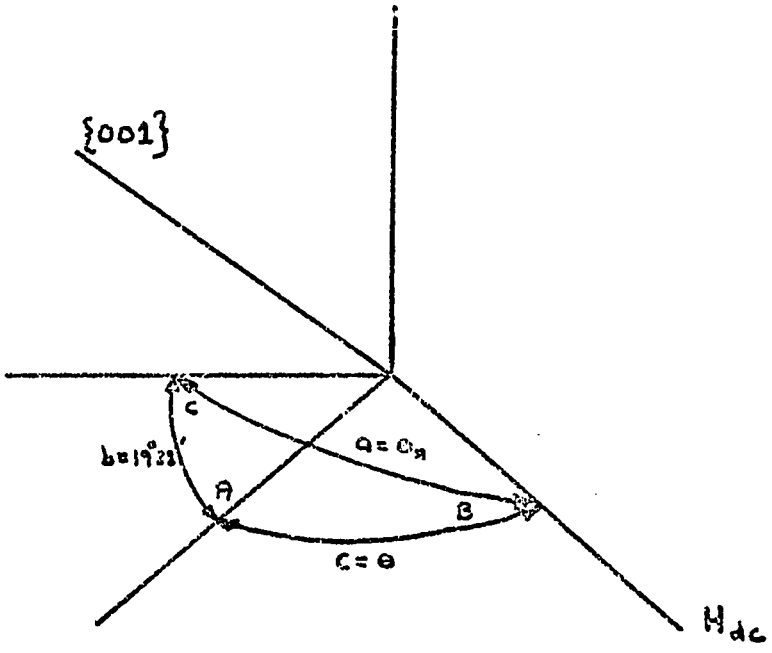

Figure 4b

Figure 4a, b Solid geometry relationships for V^{3+} ions in $CsAl(SO_4)_2 \cdot 12H_2O$. In Figure 4a H_{dc} moves in a {111} plane.

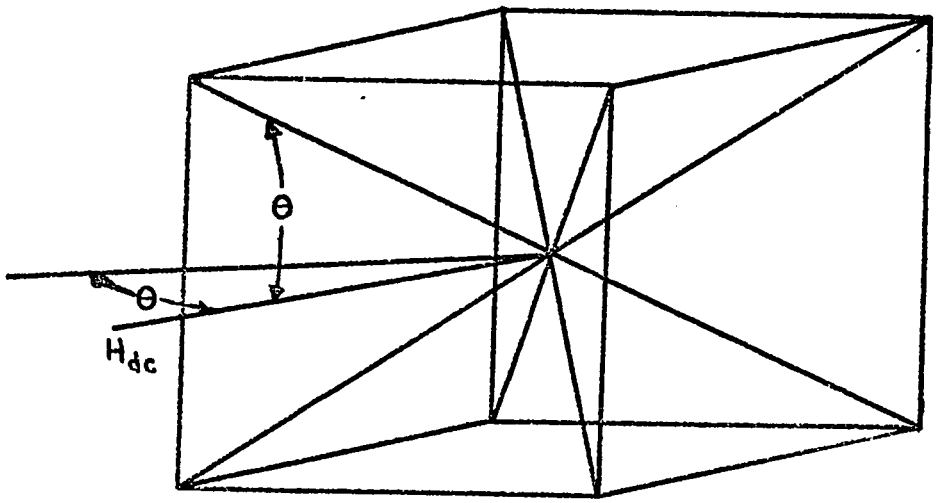

Figure 5a

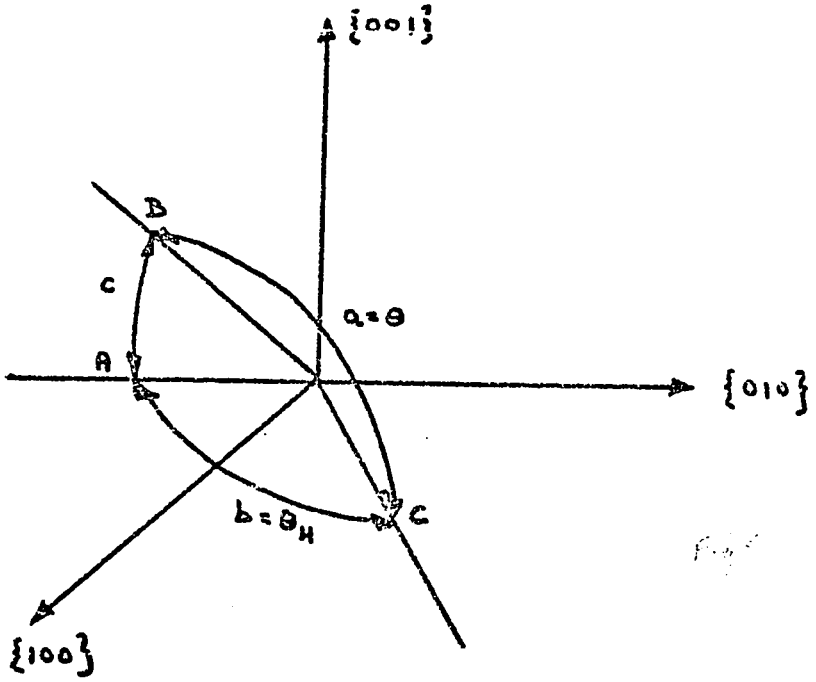

Figure 5b

Figure 5a,b Solid geometry relationships for V^{3+} ions in $CsAl(SO_4)_2 \cdot 12H_2O$. In Figure 5a H_{dc} moves in a {100} plane.

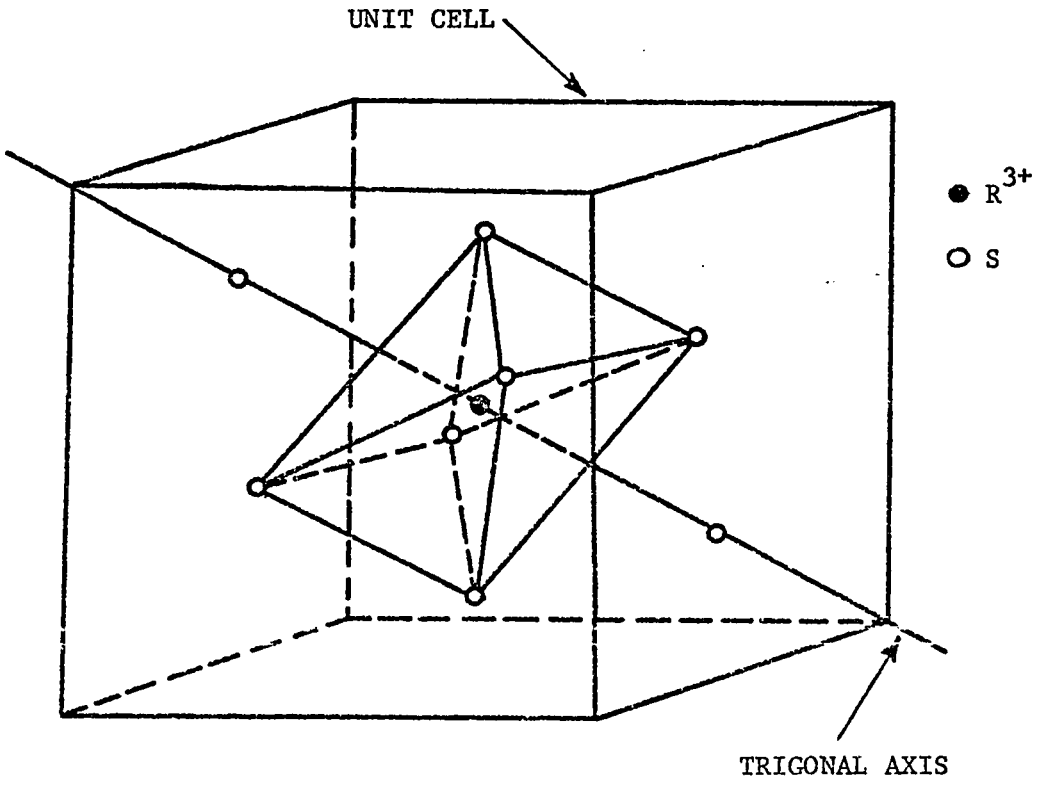

Figure 6. The second-neighbor sulfur atoms are presented as forming a trigonally distorted octahedron which surrounds R^{3+}. Outside of this octahedron and on the axis of trigonal symmetry lie the fourth-neighbor sulfurs.

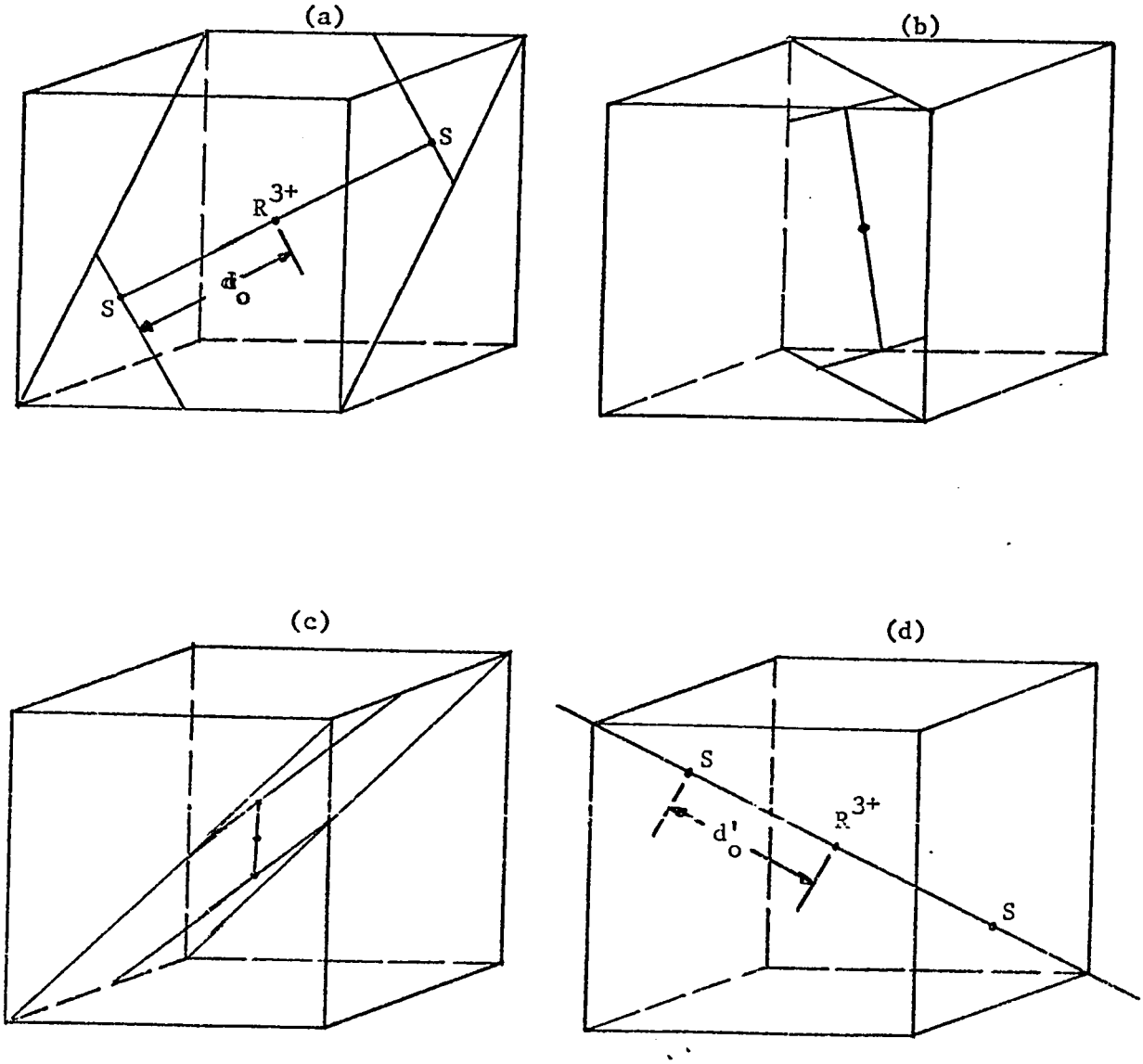

Figure 7. The locations of the eight sulfur atoms which surround R^{3+} in a unit cell are shown schematically. In (a) through (c), the three pairs of second-neighbor sulfurs are presented as lying in {110} planes at the intersections of [111] axes in their respective octants and the line approximately perpendicular to these axes passing through R^{3+} at the center of the unit cell. The distance from R^{3+} to each of these six S atoms is denoted by d_o. In (d), the two fourth-neighbor sulfurs are shown as lying on the main body diagonal at a distance from R^{3+} denoted by d_o'.

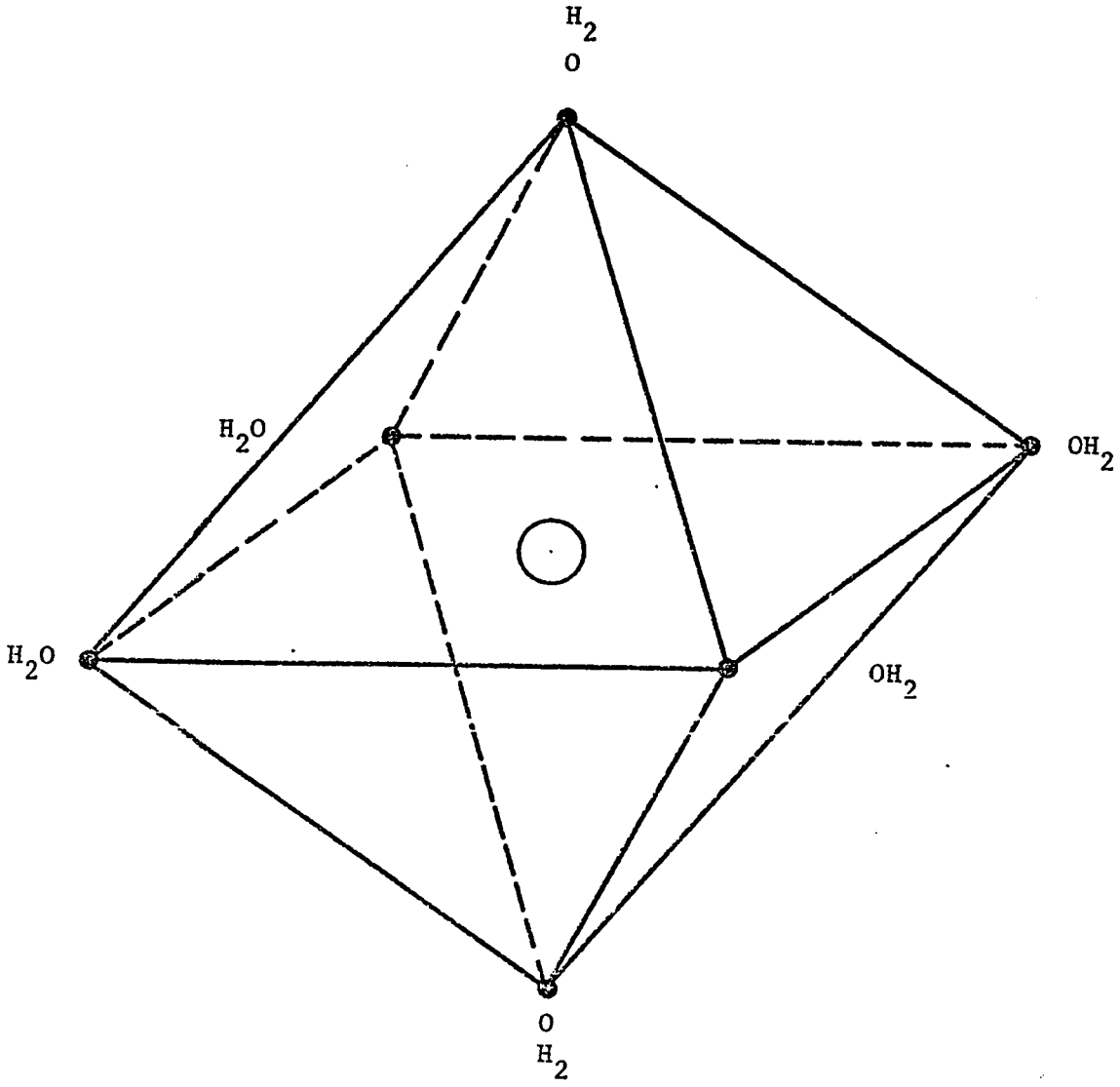

Figure 8. Octahedron of water molecules round a paramagnetic 3d ion.

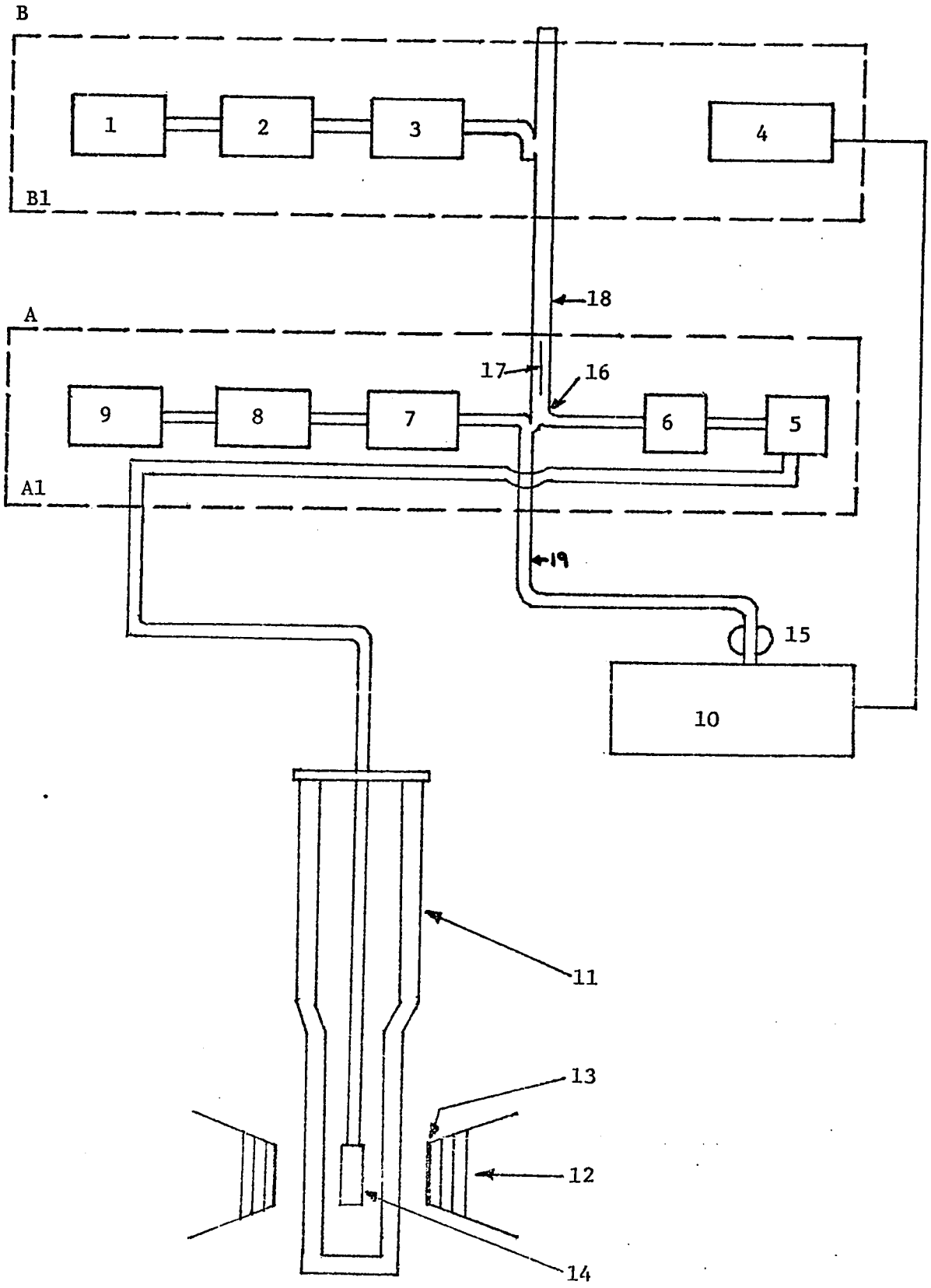

Figure 9. Block diagram of Electron Spin Resonance Apparatus.

Reference for Figure 9

Components of the functional block diagram

A	Varian X-band Microwave Bridge V-4500-42
A1	Bridge Case
B	Varian X-band Superheterodyne Adapter V-4554-1
B1	Adaptor case
1	Klystron local Oscillator
2	Ferrite isolator
3	Variable attenuator
4	30 MHz IF amplifier and second detector
5	Phase Shifter
6	Croystat isolator
7	Variable attenuator
8	Ferrite isolator
9	Klystron
10	Pre-amplifier
11	Dewar system
12	Direct Current magnet
13	Modulation coils
14	Sample cavity
15	Crystal detector tuner
16	Hybrid junction
17	Slidescrew tuner
18	High power arm
19	Detector arm

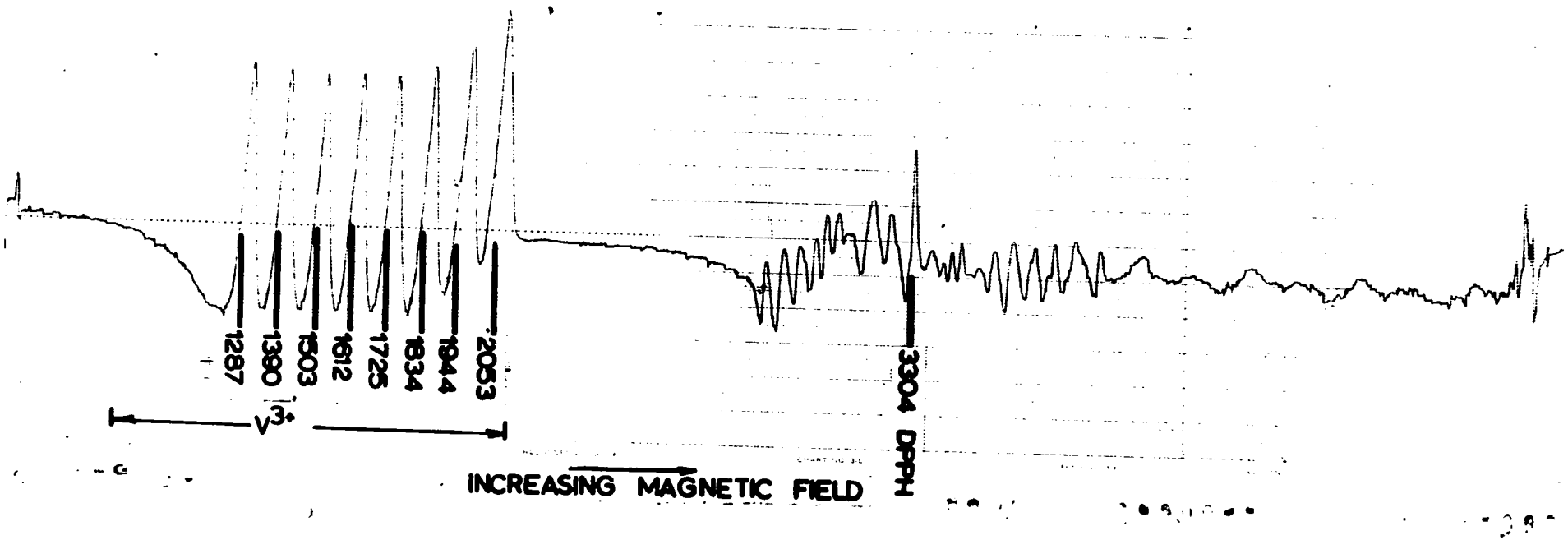

Figure 10. A recorder trace of the derivative of power absorbed by the V^{3+} ions in CsAl alum as function of the magnetic field is shown. The magnetic field direction is along a[111[direction. The temperature of the sample is $4.2^{o}K$ and the frequency of the klystron is 9270 Mc/sec. D.P.P.H. was used as a magnetic field marker. The resonance about D.P.P.H. are due to another oxidation state of the vanadium ions. The dc magnetic field is parallel to the H_{ff} for this recording

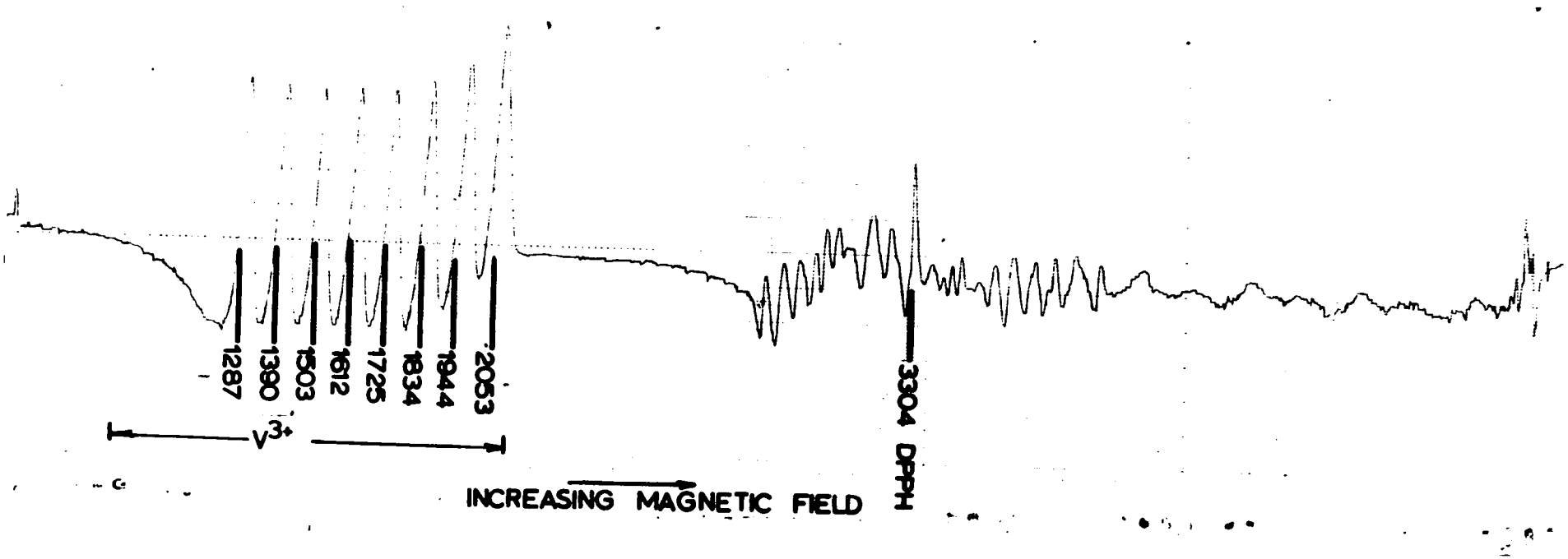

Figure 10. A recorder trace of the derivative of power absorbed by the V^{3+} ions in CsAl alum as function of the magnetic field is shown. The magnetic field direction is along a[111[direction. The temperature of the sample is $4.2^{o}K$ and the frequency of the klystron is 9270 Mc/sec. D.P.P.H. was used as a magnetic field marker. The resonance about D.P.P.H. are due to another oxidation state of the vanadium ions. The dc magnetic field is parallel to the H_{rf} for this recording

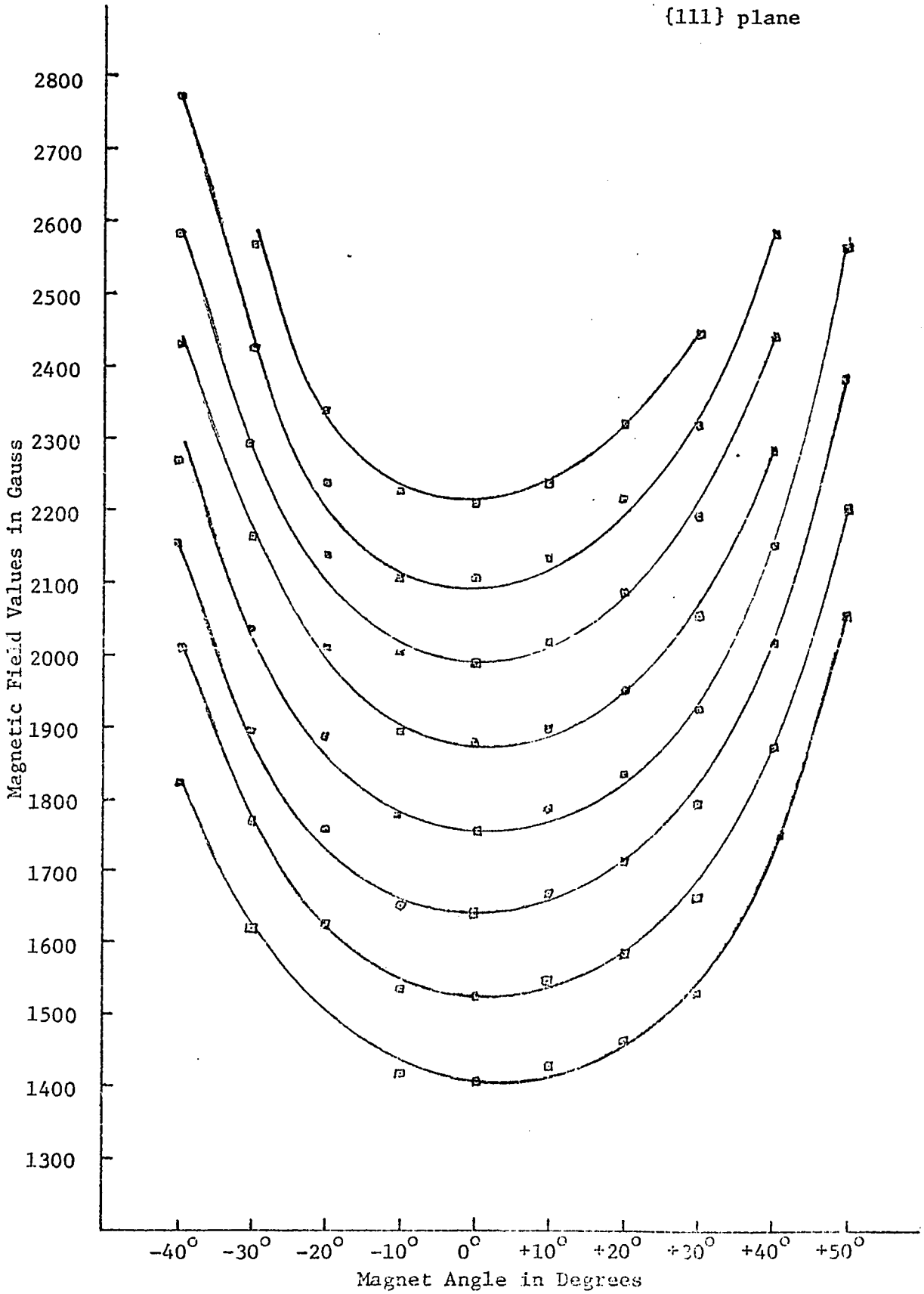

Figure 11. Resonance magnetic field variation with magnet angle.

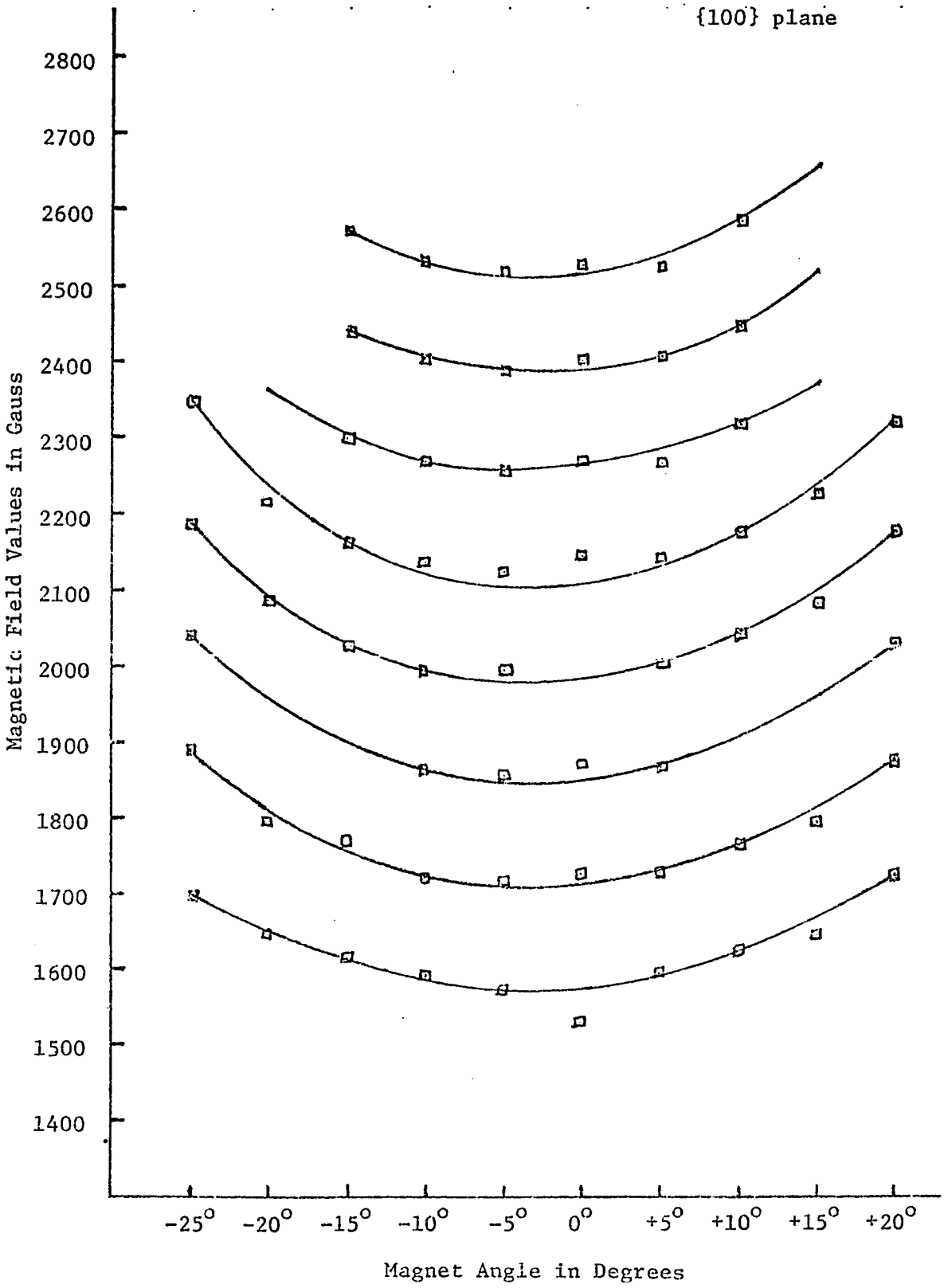

Figure 12. Resonance magnetic field variation with magnet angle.